12-1-2000

# ON THE PERSISTENCE OF SMALL REGIONS OF VORTICITY IN THE PROTOPLANETARY NEBULA

S. S. Davis
*NASA Ames Research Center*, sdavis@mail.arc.nasa.gov

D. P. Sheehan
*University of San Diego*, dsheehan@sandiego.edu

J. N. Cuzzi
*NASA Ames Research Center*, jcuzzi@mail.arc.nasa.gov

THE ASTROPHYSICAL JOURNAL, 545:494–503, 2000 December 10


# ON THE PERSISTENCE OF SMALL REGIONS OF VORTICITY IN THE PROTOPLANETARY NEBULA

S. S. DAVIS
NASA Ames Research Center, MS 260-1, Moffett Field, CA 94035; sdavis@mail.arc.nasa.gov
D. P. SHEEHAN
Department of Physics, University of San Diego, San Diego, CA 92110; dsheehan@acusd.edu
AND
J. N. CUZZI
NASA Ames Research Center, MS 245-3, Moffett Field, CA 94035; jcuzzi@mail.arc.nasa.gov
*Received 1999 October 12; accepted 2000 April 26*

## ABSTRACT

The fate of small regions of vorticity in a barotropic model of the protoplanetary nebula is investigated over thousands of years using a finite difference model. It is found that the coherence time for a small island of vorticity depends on its size, strength, orientation, and radial location in the nebula. Anticyclonic vorticity retains its coherence for longer times than cyclonic vorticity due to favorable interactions with the Keplerian shear flow. Rossby waves are generated as a result of mean vorticity gradients across the disk. The two-dimensional nebula evolves from discrete vortices into an axisymmetric flow consisting of small-amplitude vortex sheets at the radial locations of the initial vorticity. These vortex sheets induce an additional small, potential flow velocity superimposed on the Keplerian rotation curve.

*Subject headings:* accretion, accretion disks — hydrodynamics — waves

## 1. INTRODUCTION

Thin, rotating sheets of fluid are long-standing models for meteorological and oceanographic phenomena. Recently, increasing interest is being placed on these concepts for application to planetary formation and evolution. The rotating protoplanetary nebula is a thin disk that shares many physical features with the atmosphere of the rotating Earth; but there are important differences. These factors were recently investigated by Sheehan et al. (1999). Of course, the astronomical nebula theory was advanced by Laplace in 1796 and amplified by many investigators over the following two centuries, and the role of turbulence was forcefully advocated by von Weizsäcker in the 1940s (Safronov 1972). However, new insights from the atmospheric sciences in understanding large-scale turbulence and wave motions may have important applications to modeling the origin and early evolution of coherent structures in primitive solar systems. In particular, even the simplest barotropic models help to identify fundamental processes underlying the physical nature of the earth's atmosphere, its instabilities, and the formation of large-scale vortex motions (Haltiner & Martin 1957; Pedlosky 1979; Holton 1992). These phenomena may also play an important role in understanding extraterrestrial phenomena. The strong synergy between geophysical and astrophysical problems was recognized decades ago and a strong case was made then for even more interactions (Lebovitz 1983). Adams & Watkins (1995) discuss in detail the role of meteorological-type vortices in circumstellar disks. Although their local approximation does not explicitly include global shear flow effects, they clearly describe the important role of vortices in the nebula. They address the important issue of baroclinic effects on generating such vortices and speculate on the role of vortices in forming the giant planets. Barge & Sommeria (1995) investigate von Weizsäcker's hypothesis that long-lived vortices in the protoplanetary nebula play an important role in planet formation and show how an idealized vortex can capture and concentrate interplanetary dust particles.

Strongly sheared flows quickly dissipate coherent vortex structures. This fact is interesting since long-lived vortices could be a major aspect of the planet formation process. Another feature of sheared rotating fluids is that they support a type of propagating vorticity called the Rossby wave (Rossby 1945; Dickinson 1978), and these waves may also play an important role in the protoplanetary nebula.

A number of recent investigations consider the effect of shear and waves in the protoplanetary nebula and report some interesting and suggestive results. Balbus & Hawley (1998) review turbulence and angular momentum transport in accretion disks and discuss the locally acting Cartesian "shearing box" approach. However, they point out the still unfulfilled need to understand the effect of global disk geometry. In recent papers (Bracco, Chavanis, & Provenzale 1998a; Bracco et al. 1998b), transport properties of vortices in barotropic fluids are investigated with direct application to protoplanetary disks. In particular, they use a spectral-based numerical method on a Cartesian grid to study the tendency of turbulent disks to favor anticyclonic coherent vortices in decaying two-dimensional turbulence. (Anticyclonic vortices actually dominate the gas giant planetary atmospheres by a ratio of 9:1.) They show that these coherent vortices last long enough to form "lumpy structures" that may concentrate solid objects and accelerate planetesimal formation. These papers also describe the close analogy between shallow water theory and physical processes in the protoplanetary disk. This and similar work on barotropic turbulence is reviewed and related to particle aggregation and the origin of planets by Provenzale (1999). Recently, Godon & Livio (1999) extended the work to a viscous compressible nebula by simulating discrete vortices in accretion disks using related pseudospectral numerical techniques. They confirm the longer survival rate for anticyclonic vortices and show that the general behavior remains similar in a compressible flow environment.

Papaloizou & Pringle (1985) implicitly considered the

role of Rossby waves in rotating cosmological fluids as low-wavenumber instability. In a recent paper Lovelace et al. (1999) investigate the general stability of nonbarotropic disks and derive dispersion relations for Rossby wave phenomena. They consider the more complex baroclinic flow when vorticity is not conserved. Sheehan et al. (1999) discuss the analogy between meteorological and cosmological wave motions in some detail, emphasizing the fundamental role of Rossby waves in the former case, and argue that Rossby waves probably play a role in the protoplanetary nebula. In this paper, Rossby waves are revisited and found to appear as a natural outcome of the flow in a perturbed rotating flow.

Rayleigh's stability criterion states that an axisymmetric rotating flow with radially increasing angular momentum is stable and small perturbations should quickly dissipate. The rotation curve derived from Kepler's law (velocity $\sim 1/r^{1/2}$) is extremely stable based on the Rayleigh criterion. One remaining outstanding issue regards the stability of nonaxisymmetric coherent structures in such a highly sheared flow. The recent investigations cited above showed that both large-scale coherent structures and symmetry-breaking wave motions may indeed occur in the protoplanetary nebula. The present work shows that longer time evolution of these coherent structures can lead to large-scale radially variable perturbations to the baseline Keplerian rotation curve, thus potentially contributing to global rearrangement of the nebular structure. Another related issue is the underlying mechanism forming such large-scale structures. The tendency of disks with an initial random vorticity field to evolve into coherent vortices is one way (Bracco et al. 1998a). Another possibility is that discrete events such as massive clumpy infall from the surrounding cloud will strongly affect the otherwise quiescent disk. In either case, a local vortex structure will form, and questions arise regarding the fate of such vortices.

Bracco et al.'s (1998b) simulations motivate the current work. Their paper modeled a nebula using a periodic Cartesian grid with imposed larger scale vorticity and investigated the effect of vortex merging. Here we consider smaller scale discrete vortices and their role in generating long-range Rossby waves. This smaller scale vorticity is controlled by the local shear rate as far as vortex stretching is concerned and by the vorticity gradient as far as Rossby wave generation is concerned. In contrast with Bracco et al.'s large vortices, the physical effects are more apparent with a vortex that is typical of the size and rotation rate of the outer planets.

In this paper we consider the evolution of a compact region of coherent vorticity, and the associated Rossby wave, in the protoplanetary nebula from a global point of view. The fate of a test vortex in a sheared Keplerian rotating disk is simulated using the inviscid barotropic equations of motion on a polar coordinate system. A low-dispersion finite difference algorithm based on that used in acoustic wave problems (Davis 1991) tracks the vorticity field on a model nebula extending from 3 to 10 AU and timescales to 1500 yr, corresponding to 300 and 50 revolutions at $r = 3$ and 10 AU, respectively. The equations possess no explicit dissipation, so the vorticity field will not decay by the action of molecular or turbulent viscosity. The vorticity (and its associated velocity) distribution in spacetime is constrained only by the global conservation laws relating to kinetic energy and vorticity (Holton 1992, p. 972).

Bracco et al. (1998b) and Godon & Livio (1999) explicitly include viscous damping in their simulations. For example, the latter paper showed that the vortex strength decreased exponentially (about 25% after 10 orbits) for an incompressible flow model. Our simulations show that the total kinetic energy of the flow changed only by about 2% after 300 revolutions of the inner boundary. The final steady state configuration for this flow was not a simple vortex-free Keplerian flow but an axisymmetric vortex sheet with a small discontinuity superimposed on the Keplerian flow. Similar inviscid final state vortex sheets in simple shear flows were discussed by Sommeria, Staquet, & Robert (1991) in the context of two-dimensional shear layers. Of course, such final steady state flows are not actual physical entities, but the critical flow transients are tracked and illustrate the essentially inviscid fluid mechanics of the phenomenon.

Solutions obtained with a Keplerian rotation curve are contrasted with one based on a vorticity-free rotation curve. This comparison clearly shows that Rossby waves are only supported by baseline flows with nonvanishing vorticity gradients. The longer term (thousands of years) effect of rotation and shear is to redistribute the initially concentrated vorticity into meridional zones of vortex sheets with a small vortex-induced potential flow velocity extending over the entire disk. If the rotation curve possesses a vorticity gradient, Rossby waves redistribute a small portion of the initial concentrated vorticity over the entire nebula. Rossby waves are an essentially inviscid phenomenon, and the current simulations allow them to be captured over the entire disk area.

A key finding from this investigation is that the size, strength, vector orientation, and location of the vortex are all first-order determinants of its ultimate fate. A small finite vortex will quickly be sheared away by the mean velocity gradient. On the other hand, a large, strong anticyclonic vortex can induce enough velocity to just balance the local shear and can theoretically last forever. (Note that the anticyclonic Great Red Spot on Jupiter is many hundreds of years old.) Plausible assumptions are made regarding the size and strength of realistic nebular vortices lying between these extremes.

The plan of the paper is to first describe the finite difference algorithm used to solve the barotropic vorticity equations. Next, the effects of velocity shear and vortex characteristics (size, strength, orientation, and location) are investigated in the midradial region of a Keplerian shear flow. Transient Rossby waves are detected and contrasted with a shear flow having no vorticity gradients. The final steady state configuration is then illustrated by computing the fate of one of the test vortices to longer times.

## 2. NUMERICAL METHOD

Starting from the inviscid Euler equations, it is a straightforward procedure to derive the nonlinear vorticity transport equation for the horizontal, frictionless flow of an incompressible fluid:

$$\frac{\partial \xi}{\partial t} + \boldsymbol{V} \cdot \boldsymbol{\nabla} \xi = 0 \,, \tag{1}$$

where $\xi$ is the component of the total vorticity in the direction normal to the flow plane and $\boldsymbol{V}$ is the vector velocity. This apparently simple, but highly nonlinear, equation pro-

vides a general description for this class of two-dimensional flows (Choudhuri 1998). The equation is usually resolved into orthogonal components in a local Cartesian frame. Here we will consider cylindrical coordinates defined by unit vectors ($e_r$, $e_\theta$, $e_z$) in the conventional ($r$, $\theta$, $z$) notation. The vorticity is defined in the usual way by the curl of the vector velocity $\xi = \partial V_\theta/\partial r + V_\theta/r - \partial V_r/r\partial\theta$. Furthermore, we define a stream function $\psi$ by $\boldsymbol{V} = \boldsymbol{\nabla} \times \psi \boldsymbol{e}_z = V_r \boldsymbol{e}_r + V_\theta \boldsymbol{e}_\theta = \partial\psi/r\partial\theta \boldsymbol{e}_r - \partial\psi/\partial r \boldsymbol{e}_\theta$ from which $\xi = -\nabla^2\psi$. Equation (1) expressed in terms of $\psi$ is a complicated third-order partial differential equation that is the conventional starting point for numerical solutions of the barotropic vorticity equation (Holton 1992, p. 437). Rather than solving equation (1) directly, we use a two-step procedure. If the vorticity field at time step $n$ is denoted by $\xi^{(n)}$, a stream function is first computed from the polar Poisson equation

$$\nabla^2\psi = \frac{\partial^2\psi}{\partial r^2} + \frac{\partial\psi}{r\partial r} + \frac{\partial^2\psi}{r^2\partial\theta^2} = -\xi^{(n)} . \tag{2}$$

The velocity field ($V_r$, $V_\theta$) from the stream function calculation is used as coefficients in equation (1) to solve the first-order vorticity conservation equation which is the second step in the process:

$$\frac{\partial\xi^{(n+1)}}{\partial t} + V_r \frac{\partial\xi^{(n+1)}}{\partial r} + V_\vartheta \frac{\partial\xi^{(n+1)}}{r\partial\theta} = 0 . \tag{3}$$

In this manner the global effect of the vorticity as a forcing function for $\psi$ is converted into a lagged velocity field that transports the vorticity to the next time step. The velocity can be an externally applied flow (the linearized equations from dynamic meteorology), a self-induced motion (vortex-vortex interaction), or a combination of the two (as in this implementation). Such time-lagged methods have been used with success in computing vortex-dominated flows in a variety of fluid mechanics applications (Iwatsu et al. 1989; Davis 1989).

Boundary conditions are always critical issues for elliptic equations with Neumann (derivative) boundary conditions. The Poisson problem is especially difficult since solutions are subject to special compatibility conditions. Numerical solutions are exacerbated by this restraint, and solutions tend to slowly drift as time evolves. In this paper, solutions to equation (2) are obtained from a library routine (FISHPACK v3.1 distributed by NCAR) that solves Poisson's equation in polar coordinates. The boundary conditions are alternated between given velocities (normal derivatives of $\psi$) and Dirichlet conditions (values of $\psi$ obtained by integrating $V_r$ along the boundary). This approach seems to eliminate the solution creep that appears with straightforward Neumann conditions and is consistent with the small but nonvanishing changes in the boundary stream function induced by the vortex motion.

The second step is to solve the first-order vorticity convection equation. Conventional methods using simple finite difference formulas suffer from severe dispersion errors. These numerical artifacts can destroy the precise phase relations that need to be preserved during coherent wave motion. Davis (1991) demonstrated these deleterious effects for acoustic waves. In this paper, a higher order (fourth order in spacetime) method is used to advance the vorticity to the next time step. Each coordinate direction is treated separately in this spatially split scheme. Although stability and accuracy conditions for wave motion will allow a Courant number (speed × time step/grid size) close to unity, the global compatibility constraint from the Poisson equation required a much smaller time step.

Using this finite difference algorithm, solutions are obtained for as many as $10^5$ time steps. The computational domain is an annular disk from 3 to 10 AU with 113 equally spaced radial and 61 azimuthal mesh points. Test vortices of various sizes are placed at 3.5 and 7 AU, somewhat within and beyond the orbit of Jupiter. This choice simulates the local Keplerian shear and vorticity in the vicinity of the giant gas planets.

## 3. COMPUTATIONAL RESULTS AND DISCUSSION

Two parameters that determine the fate of a small island of vorticity in a large-scale shear flow are its size and its strength. A combined measure of size and strength is the circulation. A given circulation can support small vorticity over a large area or large vorticity over a small area. First, consider a baseline Keplerian shear flow. Some relevant properties, including nondimensional velocity and vorticity gradients, are shown in Table 1 at selected radii. The quantities are defined in the table and expressed in terms of the orbital velocity of the earth, $V_\theta = V_{\rm ref} = 2 \times 10^{-7}$ AU s$^{-1}$, and its distance from the Sun, $r_{\rm ref} = 1$ AU. (Starred quantities in Table 1 denote physical quantities.) The Keplerian circulation is included as a baseline value along with the local vorticity, velocity, and their gradients. The time measure is years. Note that on a Keplerian disk the circulation increases with radius, the vorticity gradient decays very rapidly, and the gradient of azimuthal velocity is the negative of the vorticity.

First consider a small, circular vortical region inserted into the baseline Keplerian flow at the point $r_0$, $\theta_0$. With respect to a locally defined polar coordinate system ($r'$, $\theta'$), the vortex decays exponentially with peak vorticity amplitude $a$ and length scale $l$ with the functional form $a \exp(-r'^2/l^2)$. The vortex induces a symmetric velocity field given by the expression: $al^2[1 - \exp(-r'^2/l^2)]/2r'$. Its

TABLE 1

PROPERTIES OF THE BASELINE KEPLERIAN NEBULA

| $r$ | $U$ | $\xi$ | $\Gamma$ | $dU/dr$ | $d\xi/dr$ | $t$ (yr) |
|---|---|---|---|---|---|---|
| 1.0..... | 1. | 0.5 | 6.28 | −0.5 | −0.75 | 1. |
| 3.5..... | 0.5345 | 0.0763 | 11.75 | −0.0763 | −0.03272 | 6.55 |
| 7.0..... | 0.3780 | 0.0270 | 16.62 | −0.0270 | −0.005785 | 18.52 |

NOTES.—$r = R^*/r_{\rm ref}$; $U = V^*/V_{\rm ref} = 1/\sqrt{r}$; $\xi = (\xi^* r_{\rm ref})/V_{\rm ref} = 0.5/r^{1.5}$; $\Gamma = \Gamma^*/(V_{\rm ref} r_{\rm ref}) = 2\pi\sqrt{r}$; $t = (1/2\pi)[(t^* V_{\rm ref})/r_{\rm ref}]$; $U$, $V$ = mean azimuthal velocity; $\xi$ = mean vorticity, $\Gamma$ = circulation; the subscript "ref" refers to conditions at the radius of Earth's orbit; "*" refers to physical quantities.

maximum value and location (with respect to its local core) depend on ($a$, $l$). As a specific example, consider a vortex whose circulation is the average of that of Jupiter and Saturn. Jupiter's period, $2\pi/\Omega$, is 10 hr, and its radius is 70,000 km. Using the formula $\Gamma = 2\pi\Omega r'^2$, the circulation is about $2.5 \times 10^{-10}$ AU$^2$ s$^{-1}$. The corresponding value for Saturn is $1.6 \times 10^{-10}$ AU$^2$ s$^{-1}$. (Here we are disregarding any caveats regarding particulars of planetary formation, e.g., runaway accretion, and all the planet's rotation is assumed captured from the surrounding vortex cloud.) A typical nondimensional value of the average circulation is $\Gamma^*/U_{\rm ref} r_{\rm ref} = 2 \times 10^{-10}/[(2 \times 10^{-7})(1)] \sim 10^{-3}$. A circulation of $10^{-3}$ for the small, circular vortex will be used as the baseline value.

Parameters relating to two possible vortices with this circulation are shown in Table 2, and these values will be the focus of the rest of this study. One is highly concentrated, and the other is more diffuse. The basic length scale $l$ is chosen to be consistent with the disk thickness, assumed to be 1/10–1/100 times the disk radius. Note that the diffuse vortex is about 3 times as big but only 1/9 times the amplitude of the intense vortex.

TABLE 2

LOCAL PROPERTIES OF THE TEST VORTEX

| Panel | $r_0$ | $a$ | $l$ | $\Gamma$ |
|---|---|---|---|---|
| a..... | 3.5 | ±0.1835 | 0.0417 | 0.001 |
| b..... | 3.5 | ±0.0204 | 0.1250 | 0.001 |
| c..... | 7.0 | ±0.1835 | 0.0417 | 0.001 |
| d..... | 7.0 | ±0.0204 | 0.1250 | 0.001 |

### 3.1. *Vortex Distortion in a Keplerian Nebula*

To a first approximation, a small vortex is convected by the mean flow, with vortices close to the central gravitator circulating faster. A better approximation is that predicted by barotropic vorticity convection and includes both shear flow distortion and self-induced velocity. There is a competition between these effects that strongly influences the subsequent evolution of the vortex.

This competition can be appreciated from Figure 1. The figure compares the initial velocity induced by the vorticity distributions in Table 2 with the baseline shear. This background shear is shown as lines of constant (negative) slope in the figure. The shear flow–induced velocities are shown relative to the mean velocities at $r = 3.5$ (Figs. 1*a* and 1*b*) and $r = 7$ (Figs. 1*c* and 1*d*), the slopes of each line being given by the value of the velocity gradients from Table 1. A qualitative analysis of the fate of each shear flow–vortex interaction can be inferred from the figure. An anticyclonic vortex ($a < 0$) is shown for illustration; that is, the vortex-induced velocities augment the mean shear. A cyclonic vortex will have exactly the reverse effect at the initial instant. Figure 1*a*, for example, shows that the initial maximum self-induced velocity from a smaller, stronger vortex adds significantly to the Keplerian shear. Figures 1*b* and 1*d* show that the shear velocities overwhelm the initial self-induced velocities from the weaker, more diffuse vorticity at both radial locations. Since these initial self-induced velocities represent upper bounds and can be expected to decay rapidly as the flow unfolds, the expectation is that mean shear flow distortion will dominate and the vortices will soon be stretched into streaky structures. Figure 1*c* is the only case where the self-induced velocity is

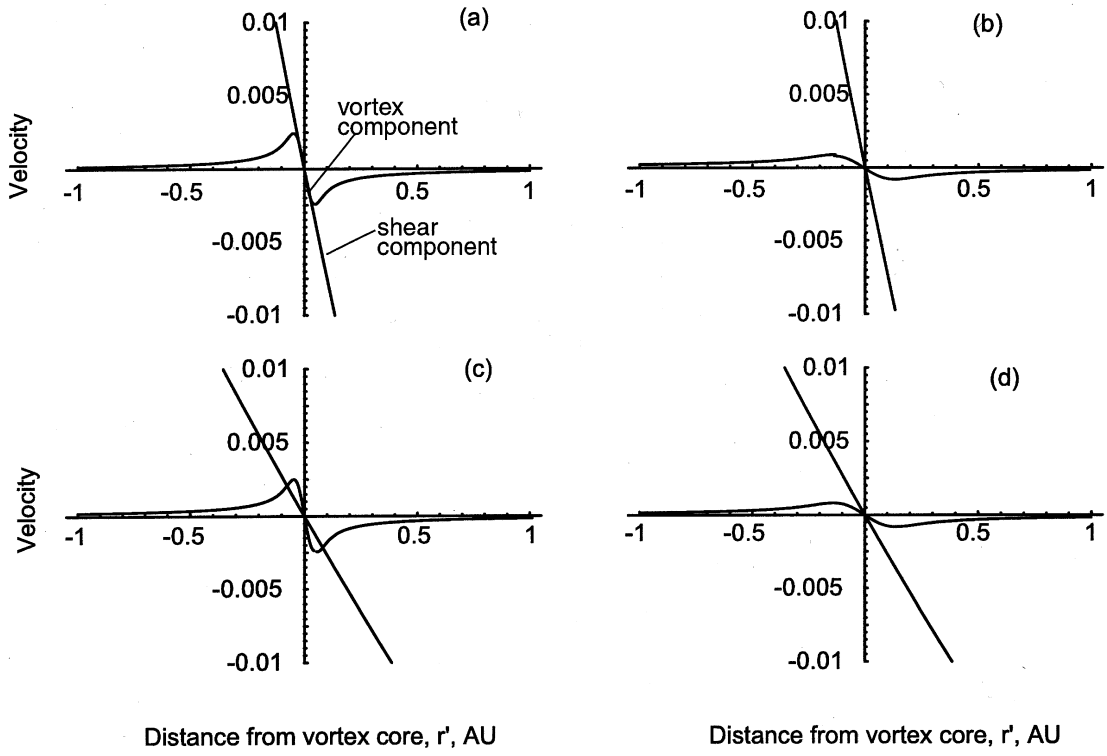


FIG. 1.—Vortex velocities compared to local Keplerian velocity gradients. (*a*) Strong, local vortex at $r = 3.5$. (*b*) Weaker, diffuse vortex at $r = 3.5$. (*c*) Strong, local vortex at $r = 7.0$. (*d*) Weaker, diffuse vortex at $r = 7.0$.

greater than the local shear-induced velocity. This is when the vorticity is concentrated in a smaller area and is located farther out radially. Finally, consider the limit case when the shear flow vanishes (horizontal line) and the self-induced velocities are all that remain. This is the classical case of nonlinear self-induced vortex motion relative to a uniform (or quiescent) mean flow. The other extreme is when the mean shear is almost vertical indicating an extremely large relative shear flow. Here the mean shear flow dominates the vorticity transport equation, the equation can be linearized, and vortices are considered point singularities. The vortex singularities just swim along with the mean current. Unlike the case of no vorticity shear (a uniformly rotating disk or a potential vortex), Keplerian shear rate curves seem capable of accommodating a wide range of shear flow–vortex interactions.

The global evolution of vorticity for cases *a–d* is shown in Figure 2 from numerical solutions of the barotropic vorticity transport equations. Snapshots of vortex convection and distortion are shown at discrete time intervals. The horizontal axis represents the periodic polar coordinate and the vertical axis the radial location from 3 to 10 AU. Each panel shows the single contour $0.25\xi_{max}$ (or $0.25\xi_{min}$), where $\xi$ is the extreme value of the disturbance vorticity at the indicated time. In all cases the initial test vortices were placed at $\theta = \pi/5$ rad and 3.5 and 7 AU as shown in the first panel. As the flow evolves, vorticity decreases and the area supporting the vorticity increases while conserving vorticity and kinetic energy. The 25% contour is representative of the vortex distortion and orientation but does not encompass the entire region of convective vorticity. Figure 2*a* shows a cyclonic case where the vorticity-induced motion aids the shearing effect. The vortices quickly become elongated (the inner vorticity moving much faster) and form streaky structures after about 200 yr. Note that a harmonic analysis of the vorticity field in the azimuthal direction would show an evolution toward lower wavenumbers (e.g., larger wavelengths) that is consistent with an energy redistribution toward lower wavenumbers. Longer time simulations show an evolution of cyclonic vorticity into elongated and overlapping streaky structures concentrated at 3.5 and 7 AU.

The contrasting case of anticyclonic vortices is shown in Figure 2*b*. Here the self-induced vorticity opposes the shearing effect of the mean Keplerian flow. This nonlinear interaction has a first-order impact on the rate of vortex distortion. The contour lines at 66 yr indicate a radial broadening and a strong reduction in the vortex shearing compared to Figure 2*a*. The effect is more dramatic at 7 AU since, from Figure 1*c*, the initial self-induced velocity is even

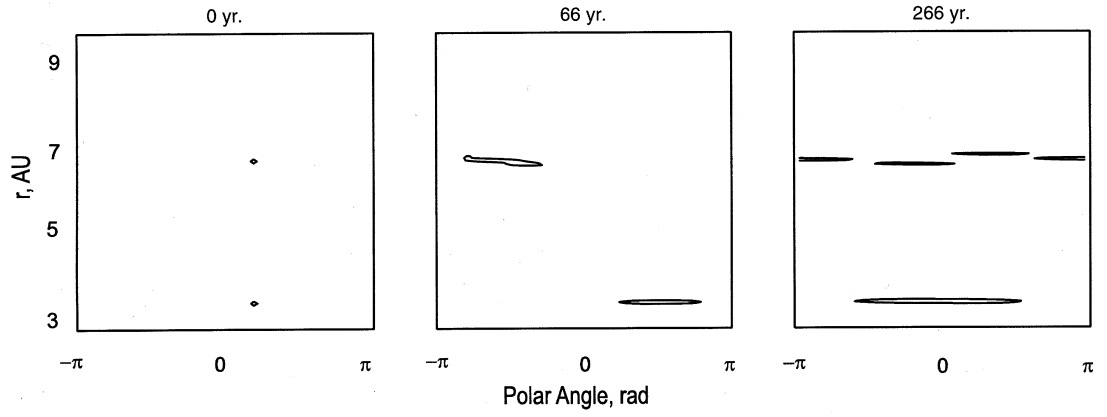


Fig. 2a

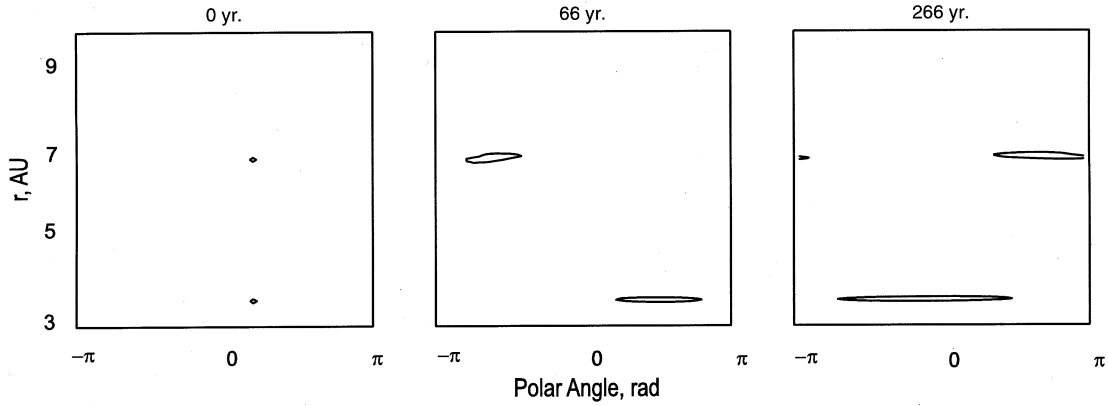


Fig. 2b

FIG. 2.—(*a*) Concentrated cyclonic vortex evolution on a thin Keplerian disk; $a = 0.1835$, $l = 0.0417$. Contours shown at $\max(\chi)/4$. (*b*) Concentrated anticyclonic vortex evolution on a thin Keplerian disk; $a = -0.1835$, $l = 0.0417$. Contours shown at $\min(\chi)/4$. (*c*) Diffuse cyclonic vortex evolution on a thin Keplerian disk; $a = 0.0204$, $l = 0.1250$. Contours shown at $\max(\chi)/4$. (*d*) Diffuse anticyclonic vortex evolution on a thin Keplerian disk; $a = -0.0204$, $l = 0.1250$. Contours shown at $\min(\chi)/4$.

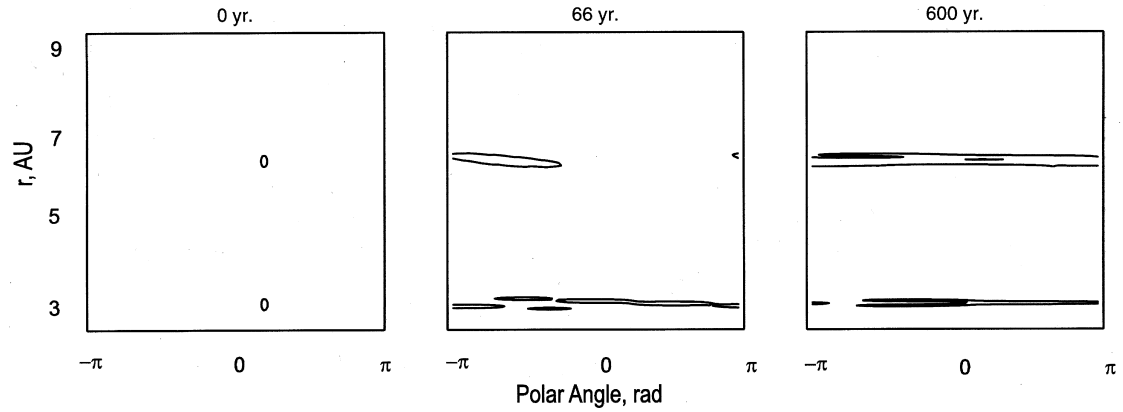


Fig. 2c

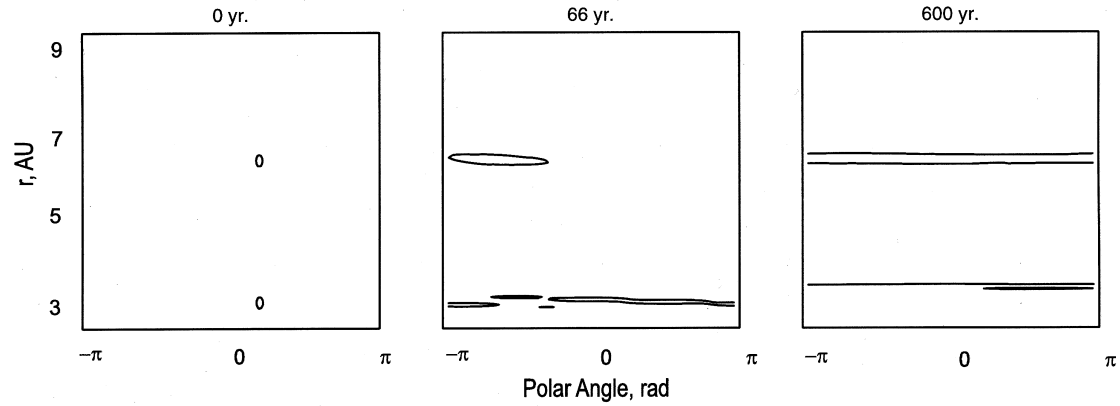


Fig. 2d

stronger than the mean shear effect. Note especially the vortex remains coherent at 266 yr compared with Figure 2*a*. The radially decreasing mean Keplerian shear rate farther out in the solar nebula is a major factor in sustaining this coherence.

Cases where the vorticity strength is severely weakened, but the core size increased to keep the circulation constant, is shown in Figures 2*c* and 2*d*. The vortex strength is about 1/9 that of the previous case, but the circulation remains constant. The effect of vorticity orientation (cyclonic or anticyclonic) is not as important as radial location. It seems that the evolution of these weaker amplitude vortices is dominated by the mean shear. This dominance is most apparent at 3.5 AU where the mean shear quickly overwhelms the vortex-induced velocities and forms continuous streaky structures at 600 yr. This flow pattern is consistent with the inviscid final states suggested by Sommeria et al. (1991).

These effects are summarized in Figure 3 depicting the approximate angular extent of the vortex as it distorts. Once the distorted shape reaches $2\pi$, the discrete nature of the vortex is eliminated in favor of a continuous azimuthal band. The time required to reach this value is a measure of the persistence of the vortex. The values were measured from contours similar to those in Figure 2. From Figures 2*c* and 2*d*, the small-amplitude, large-area vortex is overwhelmed by the local Keplerian shear at both radial locations. The base flow quickly smoothes the vortex, and nonlinear self-induction plays a minor role. Figures 3*b* and 3*d* bear this out showing small differences between cyclonic and anticyclonic vortices. The included angle reaches $2\pi$ fastest at $r = 3.5$ since the shear is greater at this station. In Figure 3*b* the discrete vortex–induced asymmetry is eliminated in about 10 local revolutions (60 yr) and in Fig. 3*d* in about 16 local revolutions (300 yr) when the data is extrapolated to $2\pi$.

The large-amplitude, smaller area vortex has a more complex evolutionary behavior pattern. Figure 3*a* indicates similar growth rates up to about 400 yr, although it was difficult to measure the exact extent of the vortex stretching from the contours. The most interesting case is at $r = 7$ (Fig. 3*c*), where the self-induction is most active. When the sense of the vortex opposes the direction of the mean shear, the cyclonic vortex rapidly shears away. The vorticity is most intense when the vortex augments the mean shear. The anticyclonic vortex persists for about 37 local revolutions (700 yr). The anticyclonic vortex also appears to have a significant lapse in growth rate between 40 and 120 yr (see also Fig. 2*b*). Also shown in Figures 3*a* and 3*c* are solid lines representing an increased angular resolution from 71 to 113 nodes. From the good agreement between the two angular resolutions, we believe that the mesh-induced numerical viscosity is extremely small and does not affect the coherence time for these vortices.

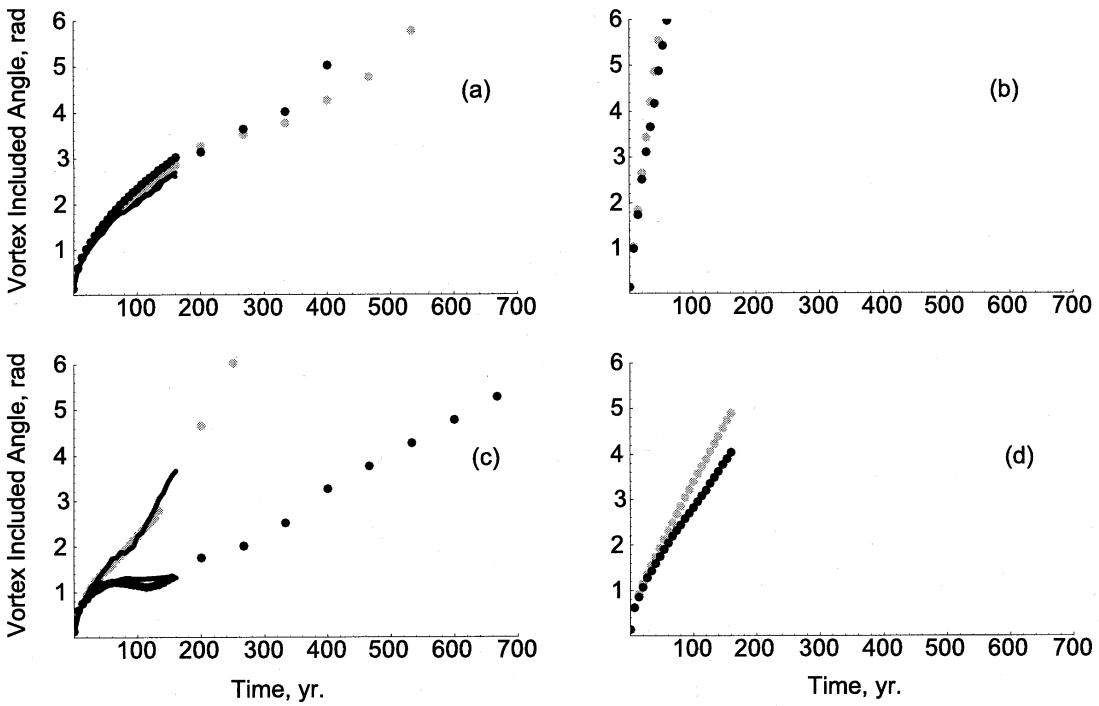


FIG. 3.—Azimuthal stretching of cyclonic and anticyclonic vorticity in the Keplerian disk. Cyclonic vortices shown as lighter circles. (*a*) Strong, local vortex at $r = 3.5$. (*b*) Weaker, diffuse vortex at $r = 3.5$. (*c*) Strong, local vortex at $r = 7.0$. (*d*) Weaker, diffuse vortex at $r = 7.0$.

These calculations indicate that physical location, strength, and size are interrelated factors that can all affect the persistence of vortices in the Keplerian flow. The examples shown here are only representative of a wide class of possible flow states. It is always possible to impose a vortex of sufficient size and strength to counterbalance the background shear and have it convect with minimal distortion for arbitrarily long times. However, vortex-induced velocities will reach moderate to high supersonic speeds, and more complex models must be considered. Initial vorticity can be induced by internal instabilities, by the cascade of turbulent energy to larger scales, or by catastrophic external events and should be the subject of additional investigations.

So far these results show that the disturbance is more or less confined to the radius where the anomalous vorticity appeared. Radial momentum and energy transfer do not play a significant role, and the main effect is to spread the disturbance by direct shearing. In the next section some longtime effects are considered showing possible radial vorticity transfer mechanisms and a longer term tendency toward zonal flows.

### 3.2. *Vorticity Waves in a Keplerian Rotation Field*

The coherence time of a local vortex was shown to depend on its associated velocity gradient. A mean vorticity gradient (not necessarily the same as the velocity gradient) is necessary to transport vorticity in the radial direction. This effect is well understood in geophysical flows where Rossby waves are described as low-frequency latitudinal excursions supported by local vorticity gradients. We expect an analogous behavior in the Keplerian rotation field. The basic mechanism is easily deduced from the barotropic vorticity transport equation. A perturbation series consisting of a mean vorticity $Z_0(r)$ and velocity $U_0(r)$, along with disturbances $\xi'(r, \theta, t)$, $u'(r, \theta, t)$, and $v'(r, \theta, t)$ are substituted in the nonlinear convection equation, equation (3). The vorticity transport equation for the perturbation is

$$\frac{\partial \xi'(r, \theta, t)}{\partial t} + U_0(r) \frac{\partial \xi'(r, \theta, t)}{r \partial \theta} + v'(r, \theta, t) \frac{\partial Z_0(r)}{\partial r} = 0 , \quad (4)$$

where $U_0$ and $v'$ are mean (azimuthal) and perturbation (radial) velocities, respectively.

This equation is well known in dynamic meteorology (Pedlosky 1979) as a prototype equation governing dispersive Rossby waves: a wave driven by the perturbed radial (latitudinal) velocity acting on a mean vorticity gradient. The general nature of Rossby waves and their relation to wavelike solutions of linear equations is reviewed in detail by Dickinson (1978). Dickinson emphases their role as theoretical building blocks in a variety of geophysical applications. A transient type of nebular wave generated by this Rossby mechanism is now discussed and contrasted with the response of a vorticity-free baseline rotation curve.

First, a surface plot of the initial vorticity (taken as the weaker, diffuse vortex) is shown in Figure 4*a* with the background mean vorticity removed. The base Keplerian rotation curve is that shown in Table 1, and the vorticity is representative of Table 2, cases *b* and *d*. As discussed previously, both initial vorticity distributions are at the same angular positions. As time evolves, the vorticity convects and stretches in the azimuthal direction. The vorticity at 33.3 yr is shown in Figure 4*b*. Aside from the main distorting vortex, a widely spaced spiral wave (marked RW in the figure) is shown in the nebular region. This Rossby wave, supported by the Keplerian vorticity gradient (increasing inward) and the induced radial velocity $v'$, spirals around the nebula with increasing pitch. The evolution of the Rossby wave for larger times is shown in the density diagrams of Figure 5. The wave spirals many times and the

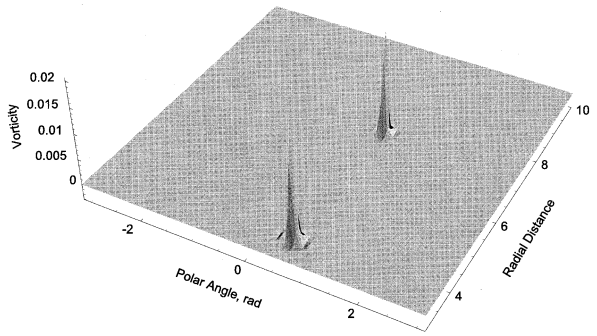


FIG. 4*a*

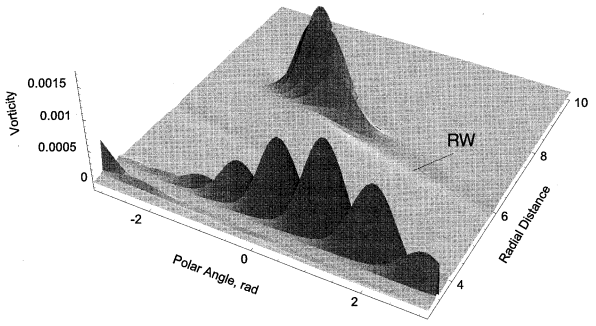


FIG. 4*b*

FIG. 4.—(*a*) Initial disturbance vorticity on a Keplerian disk. Each island of vorticity has a symmetric, exponential distribution. (*b*) Evolution of disturbance vorticity after 33.3 yr. Note faster convection and greater decay of inner vortex and presence of spiral Rossby waves.

flow reaches a quasi steady configuration after about 250 yr. The Rossby wave amplitude is just a small fraction of the stretched vorticity amplitudes at $r = 3.5$ and 7 AU (note scale on Fig. 5 is an order of magnitude less than that of Fig. 4*b*). Its amplitude is so small that numerical effects dissipate its trailing wake, and the global effect at long times is minimal. Even so, a small portion of the conserved total vortex energy is displaced radially by the Rossby wave. The initial local vortex at 3.5 and 7 AU ultimately evolves into a fully symmetric flow at larger times, and the relation between vorticity and velocity reduces to the simple axisymmetric definition of vorticity $\xi = \partial U/\partial r + U/r$.

Returning to the earlier time behavior, Figure 6 shows a surface plot (similar to Fig. 4*b*) of the vorticity convection distortion in a vorticity-free mean flow. The rotation law is now $U_0(r) = 1/r$, and the mean vorticity $Z_0(r)$ vanishes. Notice the absence of any spiral wave motion indicating that the Rossby wave generation mechanism (the last term in eq. [4]) is *not activated*. This term is the main driver (the so-called $\beta$-plane effect) behind the waves first described by

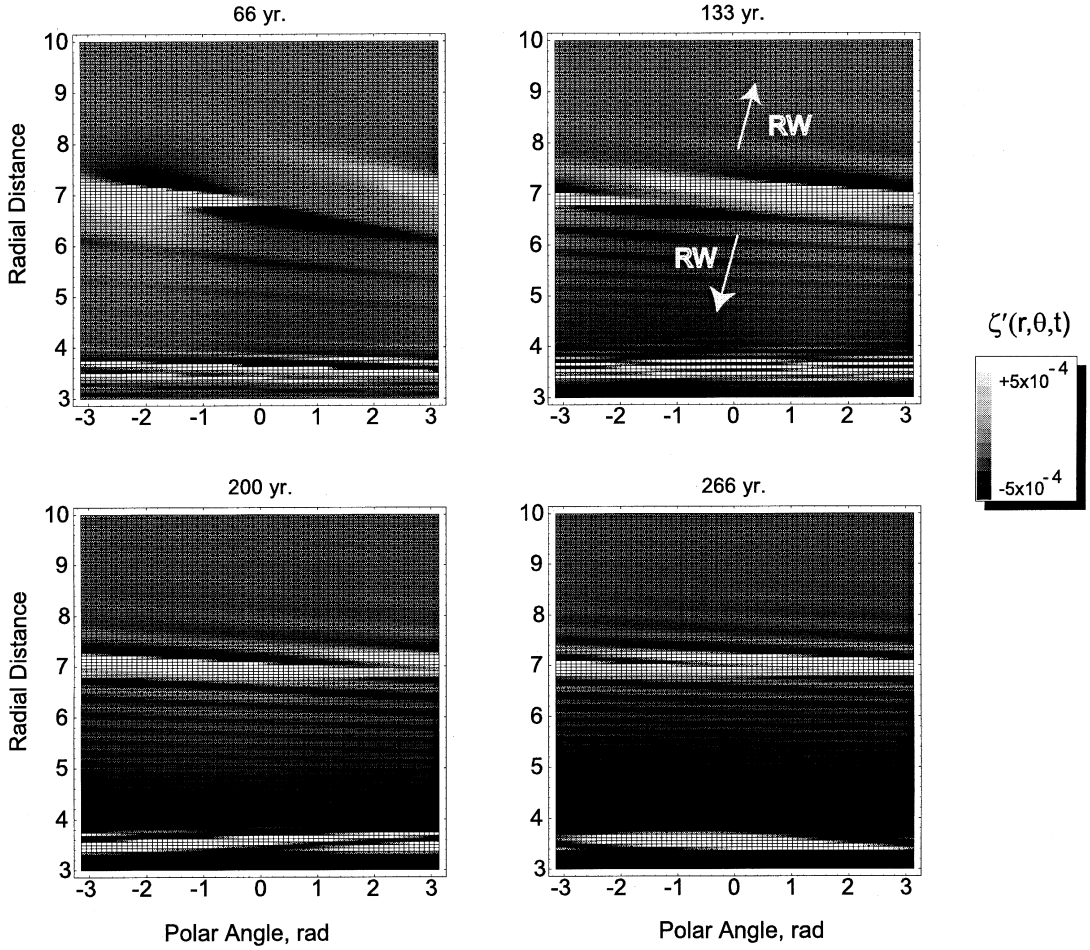


FIG. 5.—Gray-scale density plots of disturbance vorticity evolution showing increased spiraling and decay of transient nebular Rossby waves. Note decreasing amplitude as waves propagate into outer regions of nebula.

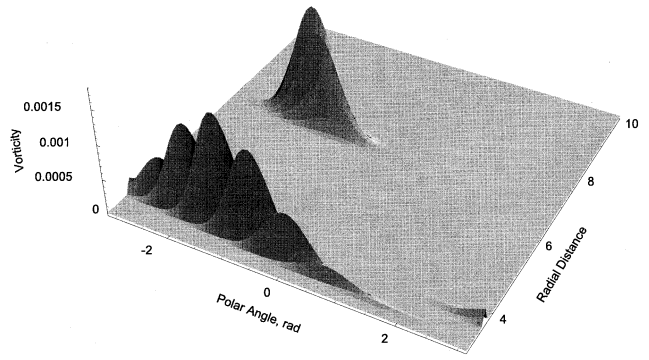


FIG. 6.—Disturbance vorticity after 33.3 yr on a disk with a potential flow background velocity rotation curve (vorticity-free flow).

Rossby (1945). The vortices shown have not convected as far as those in Figure 4*b* since the vorticity-free rotation curve ($\sim 1/r$) decreases more rapidly than the Keplerian curve ($\sim 1/r^{1/2}$).

The final state for the Keplerian rotation curve is an axisymmetric flow with discrete vortex sheets (velocity jumps) at the radial location of the initial concentrated vorticity. The evolution of the vorticity field is shown in cross section in Figure 7*a*. An earlier time radial profile of vorticity (133 yr, *solid line*) at $\theta = 0.81$ rad is compared with that at 1600 yr. (By about 1000 yr the flow is effectively axisymmetric.) The Rossby waves are indicated by the undulations in the nebula between the main vorticity spikes.

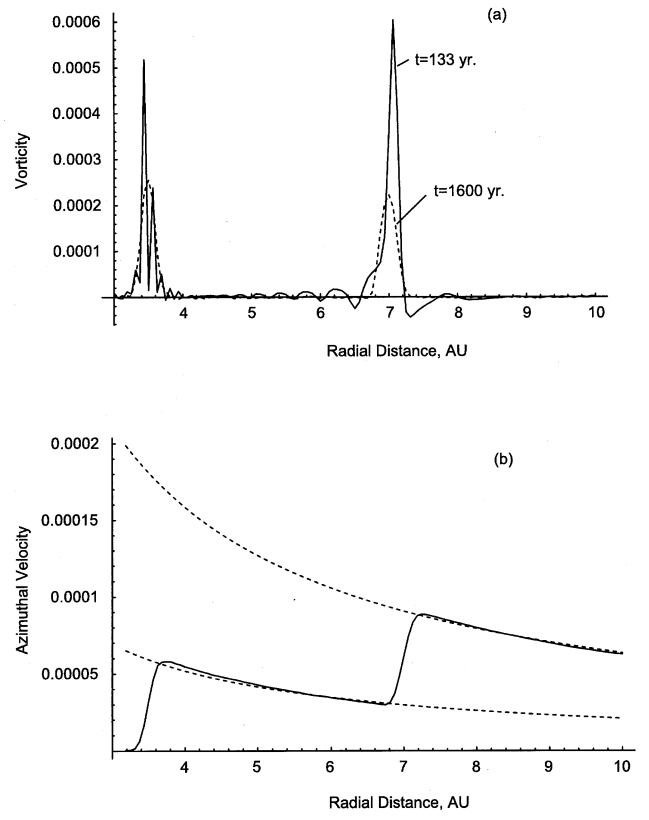


FIG. 7.—(*a*) Radial distribution of the disturbance vorticity field. At $t = 1600$ yr the vorticity is axisymmetric. (*b*) Radial distribution of the disturbance velocity field at $t = 1600$ yr. Curves of potential flow velocity, $U \sim 1/r$, shown as dashed lines.

The effect of the Rossby wave becomes inconsequential, and at longer times only the vorticity spikes are relevant.

The azimuthal velocity field can be computed from the axisymmetric vorticity using the simple relation between vorticity and azimuthal velocity given above. The final velocity field induced by a pair of cyclonic vortices is shown in Figure 7*b*. The velocity jumps are extremely small, about 0.01% and 0.014% of the local Keplerian rotation velocities at 3.5 and 7 AU, respectively. These small values are consistent with the small net circulation of the disturbance vorticity compared with the much larger Keplerian vorticity. The global effect of the vorticity is to produce an additional vortex sheet–induced velocity. Lines of $1/r$ (potential flow of an ideal fluid) are shown as dashed lines in the figure to confirm this long-reaching induced potential flow. The final state of anticyclonic vortices are just the negative of that shown in Figure 7*b*, but note that the initial transients (source of vortex persistence) are quite different in the two cases.

What is termed "final state" here will actually be modified by instabilities and three-dimensional effects. The velocity jumps, although small, are unstable to Kelvin-Helmholtz waves, and secondary instabilities will surely form. This is a natural precursor to turbulent flow in the nebula. Narrow vortex sheets are inconsistent with thin sheet, two-dimensional assumptions, and smaller scale structures will dominate in these regions. Local nonbarotropic (baroclinic) three-dimensional effects will be important. However, the induced potential flow velocities are long-range effects and are fully consistent with the underlying assumptions.

## 4. CONCLUSIONS

A barotropic model of the protoplanetary nebula was used to simulate the fate of discrete vortices in the region of the gaseous planets. A finite difference algorithm especially configured for wave propagation problems was used to compute the evolving vorticity field for several hundred orbits.

It was found that the fate of vortices depends on their size, amplitude, orientation, and location in the nebula. The competition between self-induced velocities and external shear enables the Keplerian rotation curve to support a wide variety of transient effects. The final state predicted by the model consists of discrete vortex sheets separated by a global potential flow superimposed on the base Keplerian rotation curve. Additional observations and comparative analysis of protoplanetary disks should determine appropriate scales for such coherent structures and their potential role in planetesimal formation. Some features of the structures computed here are similar to large-scale vortex structures on the giant gas planet atmospheres (Jupiter's Red Spot as a vortex whose self-induced velocity could dominate the flow pattern). Additional calculations showing particle capture over the transient lifetimes of these structures (Bracco et al. 1998a) and investigations of the narrow vortex sheet instabilities could shed light on the subsequent formation of protoplanetary bodies.

The finite difference model could be extended to include additional features. Future investigations will consider density and temperature effects, both as possible instability sources for vortex motions and as a way to model compressibility phenomena in the disk. Particle-tracking features similar to those described by Provenzale (1999) should

be incorporated. The models described here lend themselves to small-scale laboratory experiments using analogies with shallow water theory, and this approach is under active investigation. Finally, fully three-dimensional calculations of the protoplanetary nebula using finite difference techniques are definitely feasible and should be pursued.

The authors would like to thank an anonymous referee for valuable suggestions. D. P. S. was partially supported by a Cottrell College Grant from the Research Corporation. S. S. D. and J. N. C. were partially supported by an ARC DDF grant.

REFERENCES

Adams, F. C., & Watkins, R. 1995, ApJ, 451, 314
Balbus, S., & Hawley, J. 1998, Rev. Mod. Phys., 72, 1
Barge, P., & Sommeria, J. 1995, A&A, 295, L1
Bracco, A., Chavanis, P. H., & Provenzale, A. 1998a, Phys. Fluids, 11, 2280
Bracco, A., Provenzale, A., Speigel, E. A., & Yecko, P. 1998b, in Theory of Black Hole Accretion Disks, ed. M. Abramowicz, G. Björnsson, & J. Pringle (Cambridge: Cambridge Univ. Press), 254
Choudhuri, A. R. 1998, The Physics of Fluids and Plasmas (Cambridge: Cambridge Univ. Press)
Davis, S. S. 1989, in Proc. Fourth Asian Congress of Fluid Mechanics, ed. N. Ho & S. Kot (Hong Kong: Univ. Hong Kong), 157
———. 1991, J. Acoust. Soc. America, 90, 2775
Dickinson, R. E. 1978, Annu. Rev. Fluid Mech., 10, 159
Godon, P., & Livio, M. 1999, ApJ, 523, 350
Haltiner, G., & Martin, F. 1957, Dynamical and Physical Meteorology (New York: McGraw-Hill)
Holton, J. 1992, An Introduction to Dynamical Meteorology (3d ed.; New York: Academic)
Iwatsu, R., Ishii, K., Kawamura, T., Kuwahara, K., & Hyun, J. M. 1989, Fluid Dyn. Res., 5, 173
Lebovitz, N. 1983, Fluid Dynamics in Astrophysics and Geophysics (Providence: American Math Society)
Lovelace, R. V. E., Li, H., Colgate, S. A., & Nelson, A. F. 1999, ApJ, 513, 805
Papaloizou, J. C. B., & Pringle J. E. 1985, MNRAS, 213, 799
Pedlosky, J. 1979, Geophysical Fluid Dynamics (New York: Springer)
Provenzale, A. 1999, Annu. Rev. Fluid Mech., 31, 55
Rossby, C. G. 1945, J. Meteor., 2, 187
Safronov, V. 1972, Evolution of the Protoplanetary Cloud and Formation of the Earth and the Planets (Jerusalem: Israel Program for Scientific Translations)
Sheehan, D., Davis, S., Cuzzi, J., & Estberg, G. 1999, Icarus, 142, 238
Sommeria, J., Staquet, C., & Robert, R. 1991, J. Fluid Mech., 233, 661